High-resolution mapping of protein sequence-function relationships

Douglas M Fowler[1], Carlos L Araya[1], Sarel J Fleishman[2], Elizabeth H Kellogg[2], Jason J Stephany[1,3], David Baker[2,3] & Stanley Fields[1,3,4]

© 2010 Nature America, Inc. All rights reserved.

We present a large-scale approach to investigate the functional consequences of sequence variation in a protein. The approach entails the display of hundreds of thousands of protein variants, moderate selection for activity and high-throughput DNA sequencing to quantify the performance of each variant. Using this strategy, we tracked the performance of >600,000 variants of a human WW domain after three and six rounds of selection by phage display for binding to its peptide ligand. Binding properties of these variants defined a high-resolution map of mutational preference across the WW domain; each position had unique features that could not be captured by a few representative mutations. Our approach could be applied to many *in vitro* or *in vivo* protein assays, providing a general means for understanding how protein function relates to sequence.

The sequence of a protein determines its structure and function. Despite this clear correlation, understanding the relationship between protein sequence and function is a complex and largely unsolved problem. The contours of this problem have only expanded as the amount of protein sequence information, derived from DNA sequencing, has exploded. Thus, methods to rapidly couple protein sequence to protein function are needed.

One effective way to understand protein sequence-function relationships is by examining mutants. Mutational analysis has been applied both *in vitro* and *in vivo*, ranging from exploration of protein-protein interaction interfaces to analysis of the kinetics and thermodynamics of protein folding[1,2]. An example is an alanine scan, in which amino acids are individually mutated to alanine[3]. Amino acids that, when changed to alanine, result in loss or diminution of function (for example, binding, catalysis or stability) are likely of functional importance.

Mutational scanning, however, suffers from bottlenecks that have limited its utility. For example, each mutant typically needed to be cloned, expressed and purified for an *in vitro* property to be measured. The requirement to purify individual mutant proteins has been largely resolved by technologies in which a library of protein variants is linked to DNA sequences encoding the variants. Examples include protein display on the surface of phage, yeast and bacteria as well as ribosome display[4]. These enable a large pool of variants (10^6–10^{12} variants) to be assayed for a particular function in parallel. Protein display experiments generally involve multiple rounds of selection (for example, for binding) that eliminate unselected variants to yield a few highly active proteins. In addition, this scheme has been used to implement mutational scanning, including limited sampling of all possible single mutants in a short sequence[5]. Despite these advances, until recently[6–8], protein display has been limited by the requirement for Sanger sequencing of variants after selection, restricting to a few thousand the number of variants that can be examined.

Here we demonstrate that protein display using moderate selection pressure on a library of variants can be combined with high-throughput sequencing to obtain a high-resolution, fine-scale map of protein sequence-function relationships. Using the T7 bacteriophage to display over 600,000 variants of the human Yes-associated protein 65 (hYAP65) WW domain (named for its two conserved tryptophan residues)[9], we performed six rounds of selection for binding to its cognate peptide ligand. We tuned the selection parameters to produce only moderate enrichment for better binding, which maintained a large number of library members rather than converging on a few high-affinity variants. Short-read Illumina sequencing of libraries from the starting pool, and after three and six rounds of selection, enabled quantitative tracking of the fate of hundreds of thousands of variants simultaneously. The data revealed a detailed sequence-function landscape that was remarkably concordant with known WW domain features. We observed strong agreement between mutational preferences and evolutionary conservation in the WW domain. Furthermore, we comprehensively addressed the question of how mutations impair protein function. The effectiveness of moderate selection combined with high-throughput sequencing encourages a shift toward carrying out protein functional screens in a highly parallel fashion, which may reveal new aspects of protein function in many *in vitro* and *in vivo* contexts.

[1]Department of Genome Sciences, University of Washington, Seattle, Washington, USA. [2]Department of Biochemistry, University of Washington, Seattle, Washington, USA. [3]Howard Hughes Medical Institute, Seattle, Washington, USA. [4]Department of Medicine, University of Washington, Seattle, Washington, USA. Correspondence should be addressed to S.F. (fields@u.washington.edu).

RECEIVED 25 MARCH; ACCEPTED 13 JULY; PUBLISHED ONLINE 15 AUGUST 2010; DOI:10.1038/NMETH.1492

Petitioner Merck, Ex. 1151, p. 741
Merck Sharp & Dohme LLC v. Halozyme Inc.
PGR2025-00050

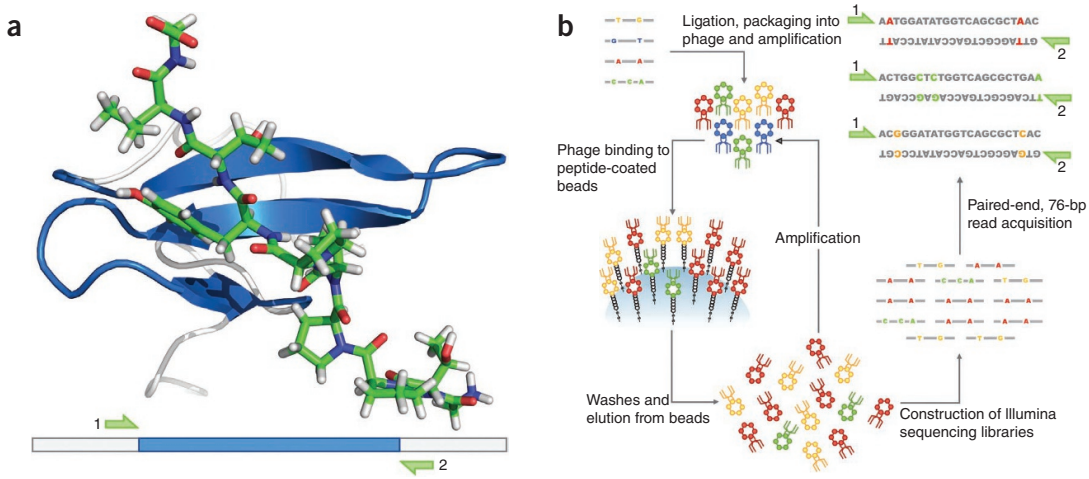

Figure 1 | A highly parallel assay for exploring protein sequence-function relationships. (**a**) PyMOL software–generated cartoon of the NMR spectroscopy structure of the hYAP65 WW domain (Protein Data Bank identifier 1jmq) in complex with its peptide ligand[16]. The portion of the mutagenized region of the hYAP65 WW domain whose encoding DNA was sequenced is shown in blue. Arrows indicate locations of sequencing primers. (**b**) A library of sequences encoding variant WW domains was generated using chemical DNA synthesis with doped nucleotide pools, PCR-amplified and displayed as a fusion to T7 capsid protein. The input phage library was subjected to successive rounds of selection. Each round consisted of phage binding to peptide ligand immobilized on beads, washing to remove unbound phage, and elution and amplification of bound phage. Sequencing libraries were created using PCR from input phage and from phage after three and six rounds of selection, and were sequenced using overlapping paired-end reads on the Illumina platform. An example of four unique variants of differing affinity are shown in different colors. Green arrows indicate locations of sequencing primers.

© 2010 Nature America, Inc. All rights reserved.

RESULTS

WW domain display and high-throughput sequencing

WW domains comprise a large family of three-stranded β-sheet structures of ~50 amino acids[9]. These domains serve as protein-protein interaction modules, binding to one of several conserved peptide motifs (**Fig. 1a**). We displayed a WW domain because its structure has been solved and because the folding, thermodynamic stability and binding preferences of WW domains have been extensively examined[10–18]. Also, the WW domain has been used in phage display experiments[18,19].

We displayed the hYAP65 WW domain on the surface of T7 bacteriophage. T7 is a lytic phage that can display large, intricately folded proteins because displayed proteins need not cross a cell membrane[20]. We fused the WW domain at the C terminus of the phage capsid protein and expressed it at an estimated 5–15 copies of the WW domain per phage. We conducted preliminary experiments using phage-displayed wild type as well as hYAP65(W17F) and hYAP65(W39F) WW domain variants, which have diminished capacity to bind peptide[14]. Each round of selection consisted of binding of mixed populations of phage to an excess of cognate GTPPPPYTVG peptide attached to beads, removal of unbound phage by wash steps and subsequent amplification of bound phage to generate an input phage library for the next round (**Fig. 1b**). Based on previous WW domain phage display experiments, we identified conditions in which affinity differences between the wild-type WW domain and these variants were readily distinguishable[19] (**Supplementary Fig. 1**).

We generated a WW domain phage library by using chemical DNA synthesis to vary 99 bases, encoding the central 33 residues of the WW domain (**Fig. 1a**). On average, each variant contained two DNA mutations. We subjected the phage library to six successive rounds of selection against the peptide (**Fig. 1b**). Sequencing libraries, prepared using PCR, provided data corresponding to a 25-residue portion of the variable region; this length was dictated by the current 76-base limit of short-read Illumina sequencing. We did not sequence the regions encoding the remaining eight variable residues of the 33, and these regions therefore contain uncharacterized mutations; however, they are not directly involved in peptide binding (**Fig. 1a**). The sequenced region encodes 25 variable residues that span the structured region of the WW domain, including both of the conserved tryptophan residues, and encompass the binding interface (**Fig. 1a**). We acquired sequencing data for the input variant library as well as after three and six rounds of selection, with an average of 10.7 million raw reads per library (**Supplementary Table 1**).

Detection of point mutations with high fidelity in a diverse library using high-throughput sequencing poses unique challenges. Under optimal conditions, short-read Illumina sequencing has an error rate of slightly less than 1%[21], leading to one expected 'mutation' resulting from sequencing error in each 76-base sequence. Thus, sequence variants obtained only one or a few times would have a high degree of uncertainty. We overcame this problem by using Illumina paired-end sequencing to capture overlapping sequence for each 76-base read pair, resulting in an average per-base error rate of 3.33×10^{-6} (1/300,000), assuming independence between reads in a pair. This low error rate allowed us to use variants sequenced only once (**Supplementary Fig. 2**). Of the average 10.7 million raw reads per library sequenced, 8.4 million passed additional quality filtering (**Supplementary Table 1**), and we aligned them to the wild-type WW domain sequence.

The quality-filtered sequencing data from the input variant library revealed 1.2 million unique DNA variants corresponding to 602,150 unique protein variants. The observed distribution of mutations in the library was close to the expected distribution[22] (**Supplementary Fig. 3**). In the DNA, we observed all possible single and nearly all double mutants as well as a large fraction of triple mutants. Because multiple DNA mutations are required to produce certain amino acid mutations, at the protein level the

Petitioner Merck, Ex. 1151, p. 742
Merck Sharp & Dohme LLC v. Halozyme Inc.
PGR2025-00050

Table 1 | Observed and predicted mutations in the input library

	DNA			Protein		
Number of mutations	Observed	Predicted	Percentage	Observed	Predicted[a]	Percentage
0	1	1	100	1	1	100
1	225	225	100	416	500	83.2
2	24,924	24,975	99.8	32,779	120,000	27.3
3	648,853	1,823,175	35.6	328,768	18,400,000	1.79

[a]Includes stop codons.

library covered 416 of the 500 possible single mutants, 32,779 of the 120,000 possible double mutants and 328,768 of the 18.4 million possible triple mutants (**Table 1**).

Assessing sequence-function relationships in the WW domain

We compared the population of protein variants present in the input library to the populations found in the round-three and round-six libraries. We assumed that the number of times a given unique protein variant was sequenced corresponded to its abundance in the library. Thus, protein variants of better than average affinity should increase in abundance after selection and be sequenced more often and vice versa for variants of worse than average affinity. We directly compared the input library to libraries after peptide selection. We did not adjust our data based on controls in which successive rounds of amplification were applied either with no selection or with selection only for expression (but not binding) of the WW domain[23]. These controls could be performed to remove hidden, variant-derived biases and potentially make the method more robust, although they could introduce their own stochastic amplification biases.

Selection eliminated the majority of variants (**Fig. 2a**); the input library of 602,150 variants greatly exceeded the complexity of the round-three (152,656 variants) and round-six (94,606 variants) libraries. Performance in this selection experiment and codon usage did not correlate ($R^2 = 0.04$), which suggests that noncoding mutations did not substantially affect WW domain selection (**Supplementary Fig. 4**). The wild-type WW domain, which represented 25.9% of the input library, increased in abundance 1.75-fold after six rounds of selection. Overall, 97.2% of the variants observed in the input library were deleterious relative to wild type.

We examined the position-averaged effect of substitution in the WW domain by calculating for each residue in the variable region an enrichment ratio, defined as the frequency of mutations in the round-six library divided by the frequency in the input library. We identified distinct regions in the WW domain that were permissive to mutation (had high mutational frequency) and others that were intolerant to mutation (had low mutational frequency) (**Fig. 2b**). As expected, the two tryptophan residues were highly intolerant to change.

We compared mutational tolerance in our assay to the evolutionary conservation of the WW domain. The hYAP65 WW

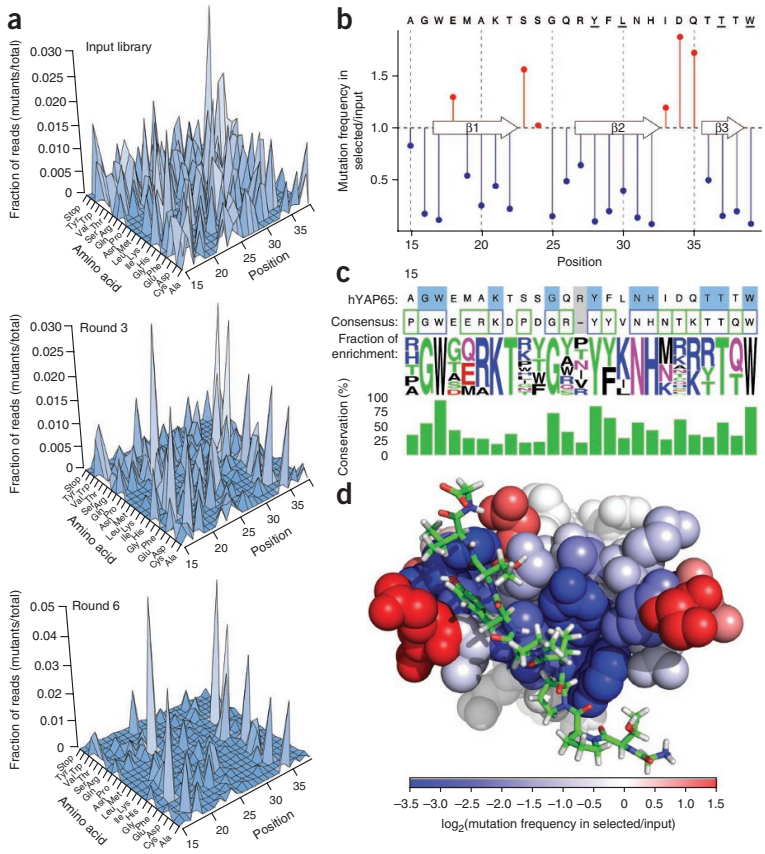

Figure 2 | Comparison of mutational tolerance and evolutionary conservation in the WW domain. (**a**) The mutational diversity of the input, round-three and round-six WW domain libraries is shown. Mutations are enumerated by position in the domain and by amino acid substitution. (**b**) Ratio of mutational frequencies in the round-six/input libraries observed at each position in the WW domain. Data for residues intolerant to mutation are shown as blue lines; data for beneficial mutations are shown as red lines. Residues making substantial contact with the peptide are underlined. (**c**) A comparison of the mutational preference at each position of the hYAP65 WW domain to a consensus WW domain sequence. Residues in the hYAP65 sequence that are identical to the consensus sequence amino acids and that were mutationally intolerant in our assay are highlighted in blue. Using mutational frequencies for enriched variants, we generated a logo plot that indicates mutational preference at each position (the plot shows only mutations that are advantageous and uses the standard coloring scheme of weblogo). Residues for which mutations to the consensus sequence were beneficial are boxed in green in the consensus sequence. The gray arginine residue is present in the hYAP65 WW domain but not in the consensus (dash). A plot of conservation is shown as a percentage of sequences in the alignment that are identical to the consensus at each position. (**d**) The mutational frequency ratio data from **b** were projected ($\log_2$-transformed) onto the space-filling model of the hYAP65 WW domain NMR spectroscopy structure (Protein Data Bank identifier 1jmq) using the PyMOL software[16]. Positions at which the frequency of mutations increased are shown in red, and positions at which the frequency of mutations decreased are shown in blue.

© 2010 Nature America, Inc. All rights reserved.

Petitioner Merck, Ex. 1151, p. 743
Merck Sharp & Dohme LLC v. Halozyme Inc.
PGR2025-00050

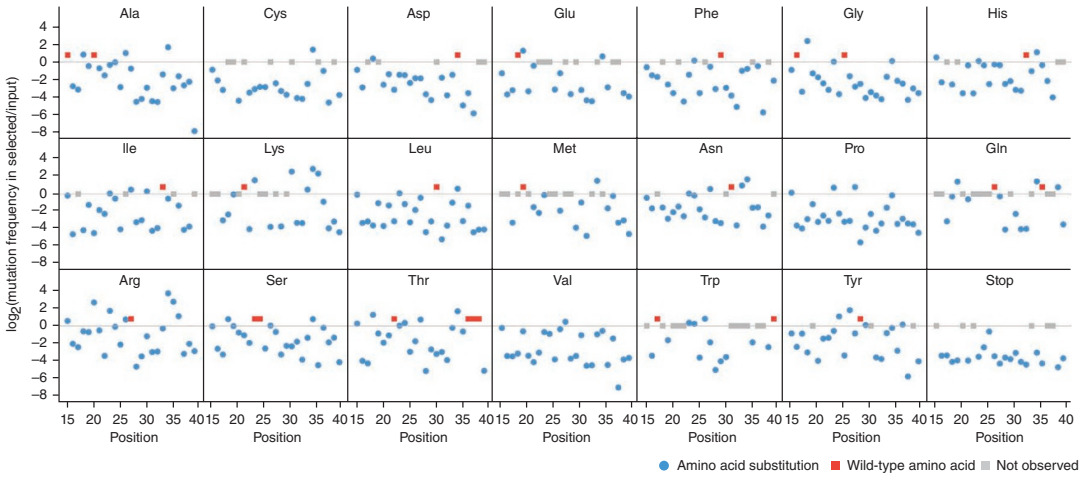

Figure 3 | Comprehensive sequence-function map of the WW domain. We calculated enrichment ratios (round-six/input libraries) for each amino acid at each position in the WW domain. Each plot corresponds to a different amino acid substitution profile as indicated. The *x* axes indicate position along the WW domain and the *y* axes indicate $\log_2$(enrichment ratio). Blue dots indicate a measured enrichment ratio and red dots indicate the wild type sequence, which enriched 1.7-fold. Gray dots indicate mutations not observed and were arbitrarily placed at zero. The alanine plot corresponds to a traditional alanine scan of the WW domain.

© 2010 Nature America, Inc. All rights reserved.

domain matches a consensus sequence generated from 72 WW domains at 11 of the 25 variable residues. Of these 11 residues, ten were intolerant of mutation in the selection experiment (**Fig. 2c**). These data are consistent with studies showing that mutation-intolerant regions *in vitro* are generally conserved in evolution[24]. Furthermore, changes in hYAP65 wild-type residues to match the consensus sequence were favorable for each of ten other residues (**Fig. 2c**). Thus, 20 of the 25 residues either remained as consensus residues or benefitted from changes to match the consensus, suggesting that our selection experiment captured general features of the WW domain evolutionary process.

Projection of the enrichment ratios onto the NMR spectroscopy structure[16] of the WW domain resulted in a spatial distribution of mutational tolerance (**Fig. 2d**). The projection showed that unlike the loop regions, the core ligand-binding region of the WW domain generally did not tolerate mutations. These findings are consistent with previous, lower-density mutational scans of the hYAP65 WW domain[17].

The high density of the data enabled us to calculate enrichment ratios for nearly every mutation in the variable region. In total, we derived enrichment ratios for 405 of the 500 possible single amino acid mutations (including mutations to stop codons) and organized these into amino acid substitution profiles comparing the round-six and input libraries (**Fig. 3**); profiles comparing round-three to input libraries were similar (**Supplementary Fig. 5a**,**b**). Additionally, the results for subsets of variants containing single or double mutations were nearly identical to those obtained with the complete set of variants (**Supplementary Fig. 5c**,**d**). These data are equivalent to an all-residue scan, in which not just alanine but each amino acid replaces the wild-type residues. Thus, these amino acid substitution profiles comprise a detailed map of sequence-function relationships for this domain.

Present in the amino acid substitution profile map are signatures of selection that delineate the effect of each amino acid when it acts as a replacement residue. For example, substitution to proline was strongly selected against at most positions, likely because prolines kink the peptide backbone and are often highly destabilizing. Substitution to cysteine, which can lead to inappropriate disulfide bond formation, was almost always deleterious. Additionally, substitution to stop codons was strongly selected against, consistent with truncated WW domains being unable to bind ligand. However, that stop codon mutations still remain after six rounds of selection puts a lower bound on the relative affinities that can be assessed.

Comparison of the amino acid substitution profiles illustrated the complexity of mutational tolerance (**Fig. 3**). Some major features were conserved among profiles, consistent with the mutationally permissive and restrictive regions of the WW domain (**Fig. 2b**). However, distinct, often radical, differences among these profiles argue that each position has a unique mutational preference (**Supplementary Fig. 6**). For example, at position 35, a change to any positively charged amino acid was beneficial. An alignment of WW domains showed that a positive charge at this position is conserved (present in 47 of 73 aligned WW domains; **Supplementary Fig. 7**). Such preferences cannot be captured by standard approaches that examine a few mutations, demonstrating the power of a high-resolution approach. In future work, we could refine the accuracy of these mutational preferences by analyzing data from sequential rounds of selection and by applying quantitative models that take into account nonspecific carryover, saturation effects and error analysis.

Comparison to published analyses

To validate our results, we searched the literature for experiments in which binding, folding or stability data had been acquired for a WW domain variant. We considered all experiments, regardless of the similarity of the WW domain analyzed to the hYAP65 WW domain. However, we excluded literature examples if the residue mutated differed from the hYAP65 WW domain residue at that position. Our search produced 72 variants that we could compare to the hYAP65 WW domain[10–18] (**Table 2**).

To eliminate the confounding effect of hYAP65 WW domain variants with multiple mutations, we compared the list of published variants to phage display enrichment ratio data only for hYAP65 variants with single amino acid mutations. We included variants that were considered significantly enriched or depleted

Petitioner Merck, Ex. 1151, p. 744
Merck Sharp & Dohme LLC v. Halozyme Inc.
PGR2025-00050

Table 2 | Comparison of the effects of WW domain mutations in this study to published results

Mutation	Agreement	Effect compared to wild type	Evidence
W17F	Yes	No structure	Thermal denaturation[11], NMR spectroscopy[14] and ITC[14]
W17Y	Yes	Worse binding	SPR analysis[17]
E18Q	Yes	Less stable	Thermal denaturation[11]
A20R	Yes	More stable	Thermal and chemical denaturation[12]
K21R	No	Better binding	Phage[18] and SPR[18] analyses
S24X	Yes (8/11)	Tolerant to any change[a]	Phage ELISA[13]
Y28L	Yes	Less stable	Thermal denaturation[11,15]
F29L	Yes	Less stable	Thermal denaturation[11]
L30K	Yes	More stable	NMR spectroscopy[16]
H32X	Yes (17/17)	Intolerant to any change[b]	Phage ELISA[13]
I33A	Yes	Less stable	Thermal denaturation[11]
D34T	Yes	More stable	Thermal and chemical denaturation[12]
Q35R	Yes	Better binding	Phage[10]
T37X	Yes (15/15)	Intolerant to any change[b]	Phage ELISA[13]
W39A	Yes	Less stable	Thermal denaturation[15]
W39F	Yes	No binding	NMR spectroscopy[14] and ITC[14]

SPR, surface plasmon resonance. ITC, isothermal titration calorimetry. ELISA, enzyme-linked immunosorbent assay.
[a]Greater than 15% binding activity. [b]Less than 15% binding activity.

© 2010 Nature America, Inc. All rights reserved.

in round six, by a Poisson distribution–based test at a 5% false discovery rate, relative to the input library (**Supplementary Fig. 8**). In our data, we found enrichment ratios for 56 of the 72 variants curated from the literature, and we used these ratios to calculate fitness values relative to the wild-type hYAP65 WW domain. We predicted that previously published mutations would be deleterious in the phage display selection if these variants had lower measured binding affinity, were thermodynamically less stable or were less structured relative to their respective wild-type versions, and beneficial if the opposite was true. The predicted effects of variants described in the literature (that is, beneficial or deleterious relative to wild type) agreed in 52 of 56 cases with the phage display fitness data (**Table 2**). This concordance highlights the ability of the phage display assay to function as an integrated measure of folding, stability and binding.

As an additional method of validation, we picked five strongly selected, singly mutated variants and tested their ability to compete with wild-type hYAP65 WW domain in the phage display assay (**Supplementary Fig. 9**). All five performed as predicted against the wild-type WW domain.

Modeling the effect of mutations on folding and binding

The phage display assay captures features of protein function such as thermodynamic stability and affinity for the ligand. To better understand the contribution of protein folding and binding to the performance of WW domain variants in the assay, we used a computational approach. For all calculations, we included full-length variants that we considered significantly enriched or depleted in round six relative to the input library, as judged by a Poisson distribution–based test at a 5% false discovery rate (**Supplementary Fig. 8**). We obtained folding energy predictions using Rosetta[25], allowing limited backbone flexibility, for these 16,363 variants. As expected, predicted folding energies were inversely related to enrichment ratios. Rosetta generally correctly predicted enriched variants as stabilized, and depleted variants as destabilized, relative to wild-type hYAP65 (Fisher's exact test, $P = 9.36 \times 10^{-84}$). These predictions were accurate for 72% of the singly and 83% of the doubly mutated variants (**Fig. 4a** and **Supplementary Fig. 10**). Predictions of more highly mutated variants agreed less frequently with experimental data (for example, 39% agreement for triply mutated variants). Rosetta-predicted stability of depleted variants was substantially less, on average, than that of the wild-type hYAP65 WW domain. We conclude that mutations that produce thermodynamic instability are the likely cause for the depletion of most variants. We also calculated binding energies for WW domain residues that have substantial contact with the ligand (Tyr28, Leu30, Thr37 and Trp39)[26]. Among protein variants with single amino acid substitutions at these residues, 69% had predicted binding energies higher than that of the wild type and highly negative enrichment ratios (**Supplementary Fig. 11**).

Single mutants predict double-mutant behavior

We used a simple product model to generate 10,192 predicted double-mutant enrichment ratios from available single-mutant data. These predicted scores had strong (Pearson's $r^2 = 0.68$) correlation with observed double-mutant enrichment ratios, showing that single-mutant behavior could generally be used to predict double-mutant behavior (**Fig. 4b**). How multiple mutations interact is an important question in protein science and evolution[27,28]. Sequencing after sequential rounds of selection would permit appropriate

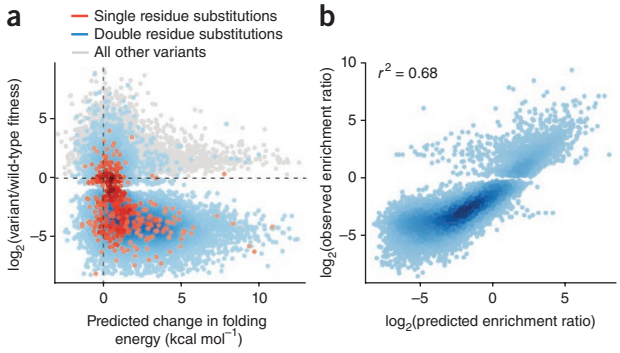

Figure 4 | Prediction of WW domain folding energies and double-mutant enrichment ratios. (**a**) The Rosetta framework was used to calculate folding energies for 16,363 full-length hYAP65 WW domain variants. Predicted folding energies relative to the wild-type WW domain energy are plotted against the observed fitness (variant/wild type) for the variants containing one, two or more mutations. (**b**) Using a basis set of single mutant enrichment ratios, we predicted double-mutant enrichment ratios using a product model.

Petitioner Merck, Ex. 1151, p. 745
Merck Sharp & Dohme LLC v. Halozyme Inc.
PGR2025-00050

correction for phage nonspecific carryover and saturation, enabling this question to be addressed quantitatively using our approach.

DISCUSSION

Our method of analyzing protein sequence-function relationships can be used to simultaneously quantify the activity of hundreds of thousands of variants of a protein. Although in the test case here we used phage display, this method could be applied to any protein functional assay in which phenotype and genotype are linked. Because the key ingredients for this approach—protein display, low-intensity selection and highly accurate, high throughput sequencing—are simple and are becoming widely available, this approach is readily applicable to many *in vitro* and *in vivo* questions in which the activity of a protein is known and can be quantitatively assessed.

For example, libraries of plasmid-encoded protein variants could be introduced into any suitable host cell or organism, followed by an appropriate selection (for example, for growth, fluorescence, transcriptional activity or other function). Sequencing of plasmids present in the populations of input and selected cells or organisms should sort the variants into functional classes. The genetic basis of disease could be explored by comprehensively profiling the functional effects of mutations on a disease-linked protein, perhaps allowing a prediction of disease progression for any newly identified cases in which this protein is affected. To guide drug treatment and development, a nearly complete map of resistance to antibiotics or anticancer drugs could be constructed by carrying out functional selections in the presence of a drug. Protein sequence-function maps could also serve to advance efforts to better understand protein evolution, folding and engineering. Ultimately, this method encourages a reimagining of the concept of protein functional screening. Moderate selection coupled with high-throughput sequencing can produce dense, fine-scale functional maps, complementing approaches that identify only a few variants with desired properties.

METHODS

Methods and any associated references are available in the online version of the paper at http://www.nature.com/naturemethods/.

Accession code. National Center for Biotechnology information Short Read Archive: SRA020603.

Note: Supplementary information is available on the Nature Methods website.

ACKNOWLEDGMENTS

We thank C. Lee and J. Shendure for assistance with DNA sequencing, and J. Kelly, J. Thomas, J. Hesselberth, E. Phizicky, A. Rubin, L. Starita and K. McGarvey for helpful comments and discussion. This work was supported by the US National Institutes of Health (P41 RR11823 to S.F. and D.B., and F32GM084699 to D.M.F.). S.F. and D.B. were supported by the Howard Hughes Medical Institute.

AUTHOR CONTRIBUTIONS

D.M.F. conceived of the method, carried out the experiments, analyzed the data and wrote the paper; C.L.A. conceived of the method, analyzed the data and wrote the paper; J.J.S. carried out the experiments; E.H.K., S.J.F. and D.B. carried out the protein folding and binding energy calculations; and S.F. conceived of the method and wrote the paper.

COMPETING FINANCIAL INTERESTS

The authors declare no competing financial interests.

Published online at http://www.nature.com/naturemethods/.
Reprints and permissions information is available online at http://npg.nature.com/reprintsandpermissions/.

1. Sidhu, S.S. & Koide, S. Phage display for engineering and analyzing protein interaction interfaces. *Curr. Opin. Struct. Biol.* **17**, 481–487 (2007).
2. Matouschek, A., Kellis, J.T. Jr., Serrano, L. & Fersht, A.R. Mapping the transition state and pathway of protein folding by protein engineering. *Nature* **340**, 122–126 (1989).
3. Cunningham, B.C. & Wells, J.A. High-resolution epitope mapping of hGH-receptor interactions by alanine-scanning mutagenesis. *Science* **244**, 1081–1085 (1989).
4. Levin, A.M. & Weiss, G.A. Optimizing the affinity and specificity of proteins with molecular display. *Mol. Biosyst.* **2**, 49–57 (2006).
5. Pal, G., Kouadio, J.L., Artis, D.R., Kossiakoff, A.A. & Sidhu, S.S. Comprehensive and quantitative mapping of energy landscapes for protein-protein interactions by rapid combinatorial scanning. *J. Biol. Chem.* **281**, 22378–22385 (2006).
6. Dias-Neto, E. *et al.* Next-generation phage display: integrating and comparing available molecular tools to enable cost-effective high-throughput analysis. *PLoS ONE* **4**, e8338 (2009).
7. Ge, X., Mazor, Y., Hunicke-Smith, S.P., Ellington, A.D. & Georgiou, G. Rapid construction and characterization of synthetic antibody libraries without DNA amplification. *Biotechnol. Bioeng.* **106**, 347–357 (2010).
8. Di Niro, R. *et al.* Rapid interactome profiling by massive sequencing. *Nucleic Acids Res.* **38**, e110 (2010).
9. Macias, M.J., Wiesner, S. & Sudol, M. WW and SH3 domains, two different scaffolds to recognize proline-rich ligands. *FEBS Lett.* **513**, 30–37 (2002).
10. Espanel, X. *et al.* Probing WW domains to uncover and refine determinants of specificity in ligand recognition. *Cytotechnology* **43**, 105–111 (2003).
11. Jager, M., Nguyen, H., Crane, J.C., Kelly, J.W. & Gruebele, M. The folding mechanism of a beta-sheet: the WW domain. *J. Mol. Biol.* **311**, 373–393 (2001).
12. Jiang, X., Kowalski, J. & Kelly, J.W. Increasing protein stability using a rational approach combining sequence homology and structural alignment: stabilizing the WW domain. *Protein Sci.* **10**, 1454–1465 (2001).
13. Kasanov, J., Pirozzi, G., Uveges, A.J. &, Kay, B.K. Characterizing class I WW domains defines key specificity determinants and generates mutant domains with novel specificities. *Chem. Biol.* **8**, 231–241 (2001).
14. Koepf, E.K. *et al.* Characterization of the structure and function of W → F WW domain variants: identification of a natively unfolded protein that folds upon ligand binding. *Biochemistry* **38**, 14338–14351 (1999).
15. Nguyen, H., Jager, M., Moretto, A., Gruebele, M. & Kelly, J.W. Tuning the free-energy landscape of a WW domain by temperature, mutation, and truncation. *Proc. Natl. Acad. Sci. USA* **100**, 3948–3953 (2003).
16. Pires, J.R. *et al.* Solution structures of the YAP65 WW domain and the variant L30 K in complex with the peptides GTPPPPYTVG, N-(n-octyl)-GPPPY and PLPPY and the application of peptide libraries reveal a minimal binding epitope. *J. Mol. Biol.* **314**, 1147–1156 (2001).
17. Toepert, F., Pires, J.R., Landgraf, C., Oschkinat, H. & Schneider-Mergener, J. Synthesis of an array comprising 837 variants of the hYAP WW protein domain. *Angew. Chem. Int. Edn Engl.* **40**, 897–900 (2001).
18. Yanagida, H., Matsuura, T. & Yomo, T. Compensatory evolution of a WW domain variant lacking the strictly conserved Trp residue. *J. Mol. Evol.* **66**, 61–71 (2008).
19. Dalby, P.A., Hoess, R.H. & DeGrado, W.F. Evolution of binding affinity in a WW domain probed by phage display. *Protein Sci.* **9**, 2366–2376 (2000).
20. Dai, M. *et al.* Using T7 phage display to select GFP-based binders. *Protein Eng. Des. Sel.* **21**, 413–424 (2008).
21. Quail, M.A. *et al.* A large genome center's improvements to the Illumina sequencing system. *Nat. Methods* **5**, 1005–1010 (2008).
22. Knight, R. & Yarus, M. Analyzing partially randomized nucleic acid pools: straight dope on doping. *Nucleic Acids Res.* **31**, e30 (2003).
23. Weiss, G.A., Watanabe, C.K., Zhong, A., Goddard, A. & Sidhu, S.S. Rapid mapping of protein functional epitopes by combinatorial alanine scanning. *Proc. Natl. Acad. Sci. USA* **97**, 8950–8954 (2000).
24. Guo, H.H., Choe, J. & Loeb, L.A. Protein tolerance to random amino acid change. *Proc. Natl. Acad. Sci. USA* **101**, 9205–9210 (2004).
25. Das, R. & Baker, D. Macromolecular modeling with Rosetta. *Annu. Rev. Biochem.* **77**, 363–382 (2008).
26. Kortemme, T. & Baker, D. A simple physical model for binding energy hot spots in protein-protein complexes. *Proc. Natl. Acad. Sci. USA* **99**, 14116–14121 (2002).
27. Bershtein, S., Segal, M., Bekerman, R., Tokuriki, N. & Tawfik, D.S. Robustness-epistasis link shapes the fitness landscape of a randomly drifting protein. *Nature* **444**, 929–932 (2006).
28. Weinreich, D.M., Delaney, N.F., Depristo, M.A. & Hartl, D.L. Darwinian evolution can follow only very few mutational paths to fitter proteins. *Science* **312**, 111–114 (2006).

© 2010 Nature America, Inc. All rights reserved.

Petitioner Merck, Ex. 1151, p. 746
Merck Sharp & Dohme LLC v. Halozyme Inc.
PGR2025-00050

ONLINE METHODS

Reagents. All chemicals were purchased from Sigma-Aldrich unless otherwise stated. Oligonucleotides were purchased from IDT with standard desalting and used without further purification unless otherwise stated. Oligonucleotides used in this study, including primers, are listed in **Supplementary Table 2**.

WW domain cloning and phage construction. Codon-optimized sequence encoding the WW domain 1 of the hYAP65 used in previous WW domain phage display experiments[19] was generated using sequential PCR with the DF-31_WWWT and DF-62_WWv2 primers. The wild-type, codon-optimized WW domain sequence was cloned into pGEM-T (Promega). The point mutants were constructed using site-directed mutagenesis with DF-106 primers (see **Supplementary Table 2** for sequences). The WW domain variant library oligonucleotide was purchased from Trilink Biosciences; the variable region was doped with 2.1% non–wild-type nucleotide (0.7% of each of the three non–wild-type nucleotides). The variant library was amplified with the WWVarV2 primers using a Platinum Taq HiFi PCR kit according to the manufacturer's instructions (Invitrogen). For cloning into the T7Select 10-3b phage display vector, Platinum Taq HiFi PCR was used to generate template. The PCR products were processed using a Qiaquick PCR cleanup kit (Qiagen) and then digested with EcoRI and HindIII (New England Biolabs). Digested fragments were purified on a 1% agarose/TBE gel and quantified by fluorescence using the PicoGreen dye (Invitrogen). The fragments were cloned into the T7Select 10-3b phage display vector and packaged into infective phage using the T7Select phage display kit following the manufacturer's instructions (Novagen/EMD Chemicals). Phage manipulation and titering were carried out following the manufacturer's instructions.

WW domain phage selection. The WW domain phage selection protocol was based on previous experiments[19]. Biotinylated GTPPPPYTVG peptide, with a disulfide linkage between biotin and peptide (bio-S-S-PPPY), at >90% purity was purchased from Anaspec and dissolved at 3 mM in deionized water. Streptavidin-coated magnetic beads (1 mg; SoluLink) were washed three times with 500 µl phage wash buffer (PWB: 25 mM Tris pH 7.2, 150 mM NaCl and 0.1% (v/v) Tween-20). The beads were then incubated in 100 µl of a 100 µM solution of the bio-PPPY peptide with mixing at room temperature (20–23 °C) for 1 h. The beads were washed three times with 500 µl of PWB and blocked for 1 h with blocking buffer (Pierce/Thermo Fisher). For each round of phage selection, amplified phage (100 µl) was added to bio-S-S-PPPY coated beads (73.5 µg or 125 pmol binding capacity) and mixed at room temperature for 1 h. The beads were washed eight times with 200 µl PWB; each wash consisted of 5 s of vortexing followed by a brief centrifugation. The bound phage were eluted in 100 µl of PWB with 20 mM dithiothreitol for 5 min. The final wash and eluate were titered, and 80 µl of the eluate was amplified. WW domain sequences were PCR-amplified and Sanger sequenced with primers DF-62_T7UPv2 and DF-62_T7DNv2 (**Supplementary Table 2**). Sanger sequencing of mixed phage populations was quantified using the PeakPicker software[29].

Illumina library preparation and sequencing. Phage library DNA was isolated by phenol-chloroform extraction and ethanol precipitation. We amplified 50 ng of phage DNA using the Phusion HF system and the DF-97_PCR_Long primers (**Supplementary Table 2**) for 15 cycles according to the manufacturer's instructions (New England Biolabs). The product was isolated using the Qiaquick PCR purification kit (Qiagen) and purified using the Ampure reagent (Beckman-Coulter). Concentrations were determined using the Quant-IT dsDNA HS kit according to the manufacturer's instructions (Invitrogen). From each library, 0.36 fmol total DNA was loaded into its own lane and sequenced using a Genome Analyzer IIx (Illumina) with the DF-97_SEQ_Short primers (**Supplementary Table 2**).

Sequence assembly and quality filtration. Sequencing data from each round as well as the input library were treated identically. An average Illumina quality score was calculated for each read in a given set of paired-end reads; read pairs in which either read had an average Phred quality score of less than 20 (99% accuracy) were discarded. Read pairs were then aligned using a global Needleman-Wunsch algorithm in the pairwise2 BioPython function (match score = 2, mismatch score = −1, gap initiation = −3, gap propagation = −1). Read-pair alignments with gaps were discarded. Surviving read pairs were merged into a single sequence, with disagreements between the read pairs being resolved in favor of the higher-quality base. Read pairs with disagreements and equal quality scores (in which discrimination between the two disagreeing bases was impossible) were discarded. DNA sequences and their amino acid translations were aligned to the wild-type WW domain sequence. Mutations were enumerated. Sequences with more than three consecutive mutations were discarded as these tended to contain obvious sequencing errors.

Calculation of mutation frequencies and enrichment ratios. We identified unique sequences (variants) from each library and computed their frequency in the library. Variants that disappeared from the input library after selection were not included. The frequency for a given variant, v, in the Xth round ($F_{v,X}$) was

$$F_{v,X} = \frac{\text{reads}_{v,X}}{\sum \text{reads}_X}.$$

We used the frequency data to compute variant enrichment ratios between successive rounds. The enrichment ratio for a given variant, v, in the Xth round ($E_{v,X}$) was

$$E_{v,X} = \frac{F_{v,X}}{F_{v,\text{input}}}.$$

Fitness scores were calculated for each variant, v, to enable comparison to wild type in the Xth round ($W_{v,X}$):

$$W_{v,X} = \frac{E_{v,X}}{E_{\text{wild type},X}}.$$

We also calculated mutation frequencies at each position for each amino acid substitution. The frequency at the ith position bearing the jth amino acid substitution in the Xth round ($F_{i,j,X}$) was

$$F_{i,j,X} = \frac{\sum \text{reads}_{i,j,X}}{\sum \text{reads}_X}.$$

© 2010 Nature America, Inc. All rights reserved.

doi:10.1038/nmeth.1492

Petitioner Merck, Ex. 1151, p. 747
Merck Sharp & Dohme LLC v. Halozyme Inc.
PGR2025-00050

We used the frequency data to compute enrichment ratios at each position for each amino acid substitution between successive rounds. The enrichment ratio at the ith position bearing the jth amino acid substitution in the Xth round ($E_{i,j,X}$) was

$$E_{i,j,X} = \frac{\sum F_{i,j,X}}{\sum F_{i,j,\text{input}}}.$$

Comparison to literature analysis. Experiments were curated from the literature in which binding, folding or stability data had been measured for a WW domain variant. For each literature variant, an expectation of enrichment or depletion, relative to wild type, was inferred. Each expectation was compared to a fitness score calculated for the relevant single mutant using Poisson filtered round-six enrichment ratios.

WW domain conservation analysis. A consensus WW domain sequence was built by alignment of 72 Pfam seed sequences of the WW domain (Pfam identifier PF00397) in Jalview using default parameters. Conservation at each position was calculated as the fraction of residues containing the consensus amino acid. Residues 173–202 of hYap65 spanning the sequenced 25 amino acid variable region were aligned to the 72 seed WW domain sequences. Amino acid mutations that increased in frequency after six rounds of selection were used to generate a logo plot in which the height of each amino acid indicates the frequency of enrichments to that residue (WebLogo; http://weblogo.berkeley.edu/).

Folding and binding energy calculations. Rosetta was used to compute binding energies between the mutant WW variants and the peptide[26] as well as the differences in folding free energies between mutant and wild type. The structure of the wild-type hYAP65 WW domain bound to the peptide (Protein Data Bank identifier 1k9q) was relaxed in several rounds of full repacking of side chains on both partners and minimization of side-chain, backbone and rigid-body degrees of freedom. In the case of binding free-energy predictions, each mutant sequence was then threaded on this model and subjected to one round of full side-chain repacking followed by side-chain, backbone and rigid-body minimization. For each sequence, the binding energy was computed 5 times and the average of that value was reported. This procedure was repeated 5 times for each mutant, and the average of these separate runs was reported. Differences in folding free energy ($\Delta\Delta G$) were performed by Rosetta (unpublished data). For both mutant and wild-type structures, all side chains were repacked followed by backbone and side-chain minimization. To ensure that the structures remained close to the starting structures, constraints were applied to all C-alpha atoms closer than 9 Å. This procedure was performed 50 times, and the predicted folding free energy is the average of the three lowest scoring structures. Rosetta scripts and command lines are available in **Supplementary Note 1**.

Prediction of double mutant behavior from single mutants. All calculations used Poisson significance-filtered round-six data. We used a product model to predict the enrichment ratio of each double mutant variant ($E_{xy,6}$) using the corresponding single mutant variant enrichment ratios ($E_{x,6}$, $E_{y,6}$):

$$E_{xy,6} = E_{x,6} \times E_{y,6}.$$

This simple model does not contain an error term (for example, to account for nonspecific carryover) and therefore should not be used to analyze epistasis.

Statistical analysis. A statistical analysis was undertaken to determine which variants changed in abundance over successive rounds of selection. A Poisson distribution was used to estimate the likelihood that the representation of each unique variant in a given round of selection had changed from the input library. *P* values were calculated by comparing the number of times each unique variant was observed in a given round of selection to the Poisson distribution based on the number of times that variant had been observed in the input library. Multiple-testing correction was performed using false discovery rate control[30].

Fisher's exact test was applied to determine whether variants were accurately classified in a contingency table with categories for variants more or less active than wild type, and predicted to be more or less stable than wild type.

29. Ge, B. *et al.* Survey of allelic expression using EST mining. *Genome Res.* **15**, 1584–1591 (2005).
30. Storey, J.D. & Tibshirani, R. Statistical significance for genomewide studies. *Proc. Natl. Acad. Sci. USA* **100**, 9440–9445 (2003).

© 2010 Nature America, Inc. All rights reserved.

doi:10.1038/nmeth.1492

Petitioner Merck, Ex. 1151, p. 748
Merck Sharp & Dohme LLC v. Halozyme Inc.
PGR2025-00050

nature | methods

High-resolution mapping of protein sequence-function relationships

Douglas M Fowler, Carlos L Araya, Sarel J Fleishman, Elizabeth H Kellogg, Jason J Stephany, David Baker & Stanley Fields

Supplementary figures and text:

Supplementary Figure 1	**Titering and Sequencing of Phage Display of the WW Domain.**
Supplementary Figure 2	**Overlapping Paired End Reads Reduce Average Error.**
Supplementary Figure 3	**Sequencing of the WW Domain Diversity Library Reveals the Expected Distribution of DNA Mutations.**
Supplementary Figure 4	**WW Domain Enrichment Ratio and Codon Adaptation Index are Uncorrelated.**
Supplementary Figure 5	**Variants Behave Similarly Across Rounds of Selection and Mutational Distance.**
Supplementary Figure 6	**Mutational Preferences by Position.**
Supplementary Figure 7	**Sequence Alignment of 73 WW Domains.**
Supplementary Figure 8	**Poisson-based Filtration of Enrichment Ratios.**
Supplementary Figure 9	**Validation of Five Singly Mutated WW Domain Variants.**
Supplementary Figure 10	**Prediction of WW Domain Folding Energies for Enriched and Depleted Variants.**
Supplementary Figure 11	**Prediction of Binding Energies for Variant WW Domains.**
Supplementary Table 1	**Results of Quality Filtration on Raw Illumina Data.**
Supplementary Table 2	**Primers and DNA Sequences.**
Supplementary Note 1	**Rosetta Scripts.**

Nature Methods: doi: 10.1038/nmeth.1492

Supplementary Figure 1. Titering and Sequencing of Phage Display of the WW Domain.

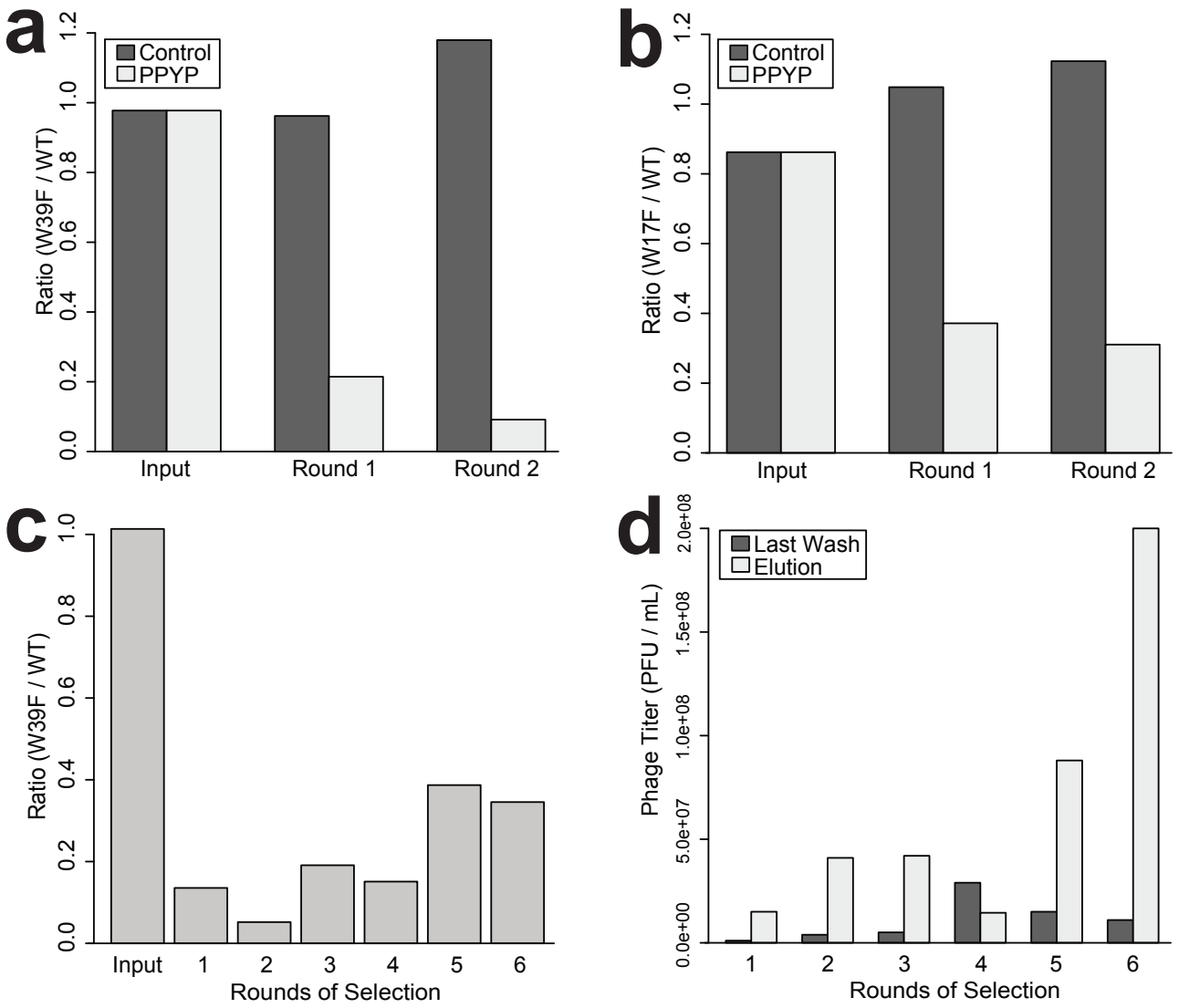

(**a**,**b**) In order to validate our phage display assay we employed two well-studied WW domain variants, W17F and W39F. Shown is quantitative Sanger sequencing data for two successive rounds of selection of each of these variants versus wild type WW domain on both control (dark gray bars) and PPYP ligand-containing (light gray bars) beads. The input phage stock contained an equal mixture of wild type and variant phage. Control beads (dark gray bars) showed no preference for either variant versus wild type. (**c**) Shown is quantitative Sanger sequencing of a control selection performed at the same time as the six round WW domain diversity library selection using identical beads and phage stocks. The input for this control selection at each round was an equal mixture of wild type and W39F. Thus, this control gives a measure of the relative strength of selection for each round. (**d**) Shown is the phage titer for the last wash and the elution after each round of selection of the WW domain diversity library.

Nature Methods: doi: 10.1038/nmeth.1492

Supplementary Figure 2. Overlapping Paired End Reads Reduce Average Error.

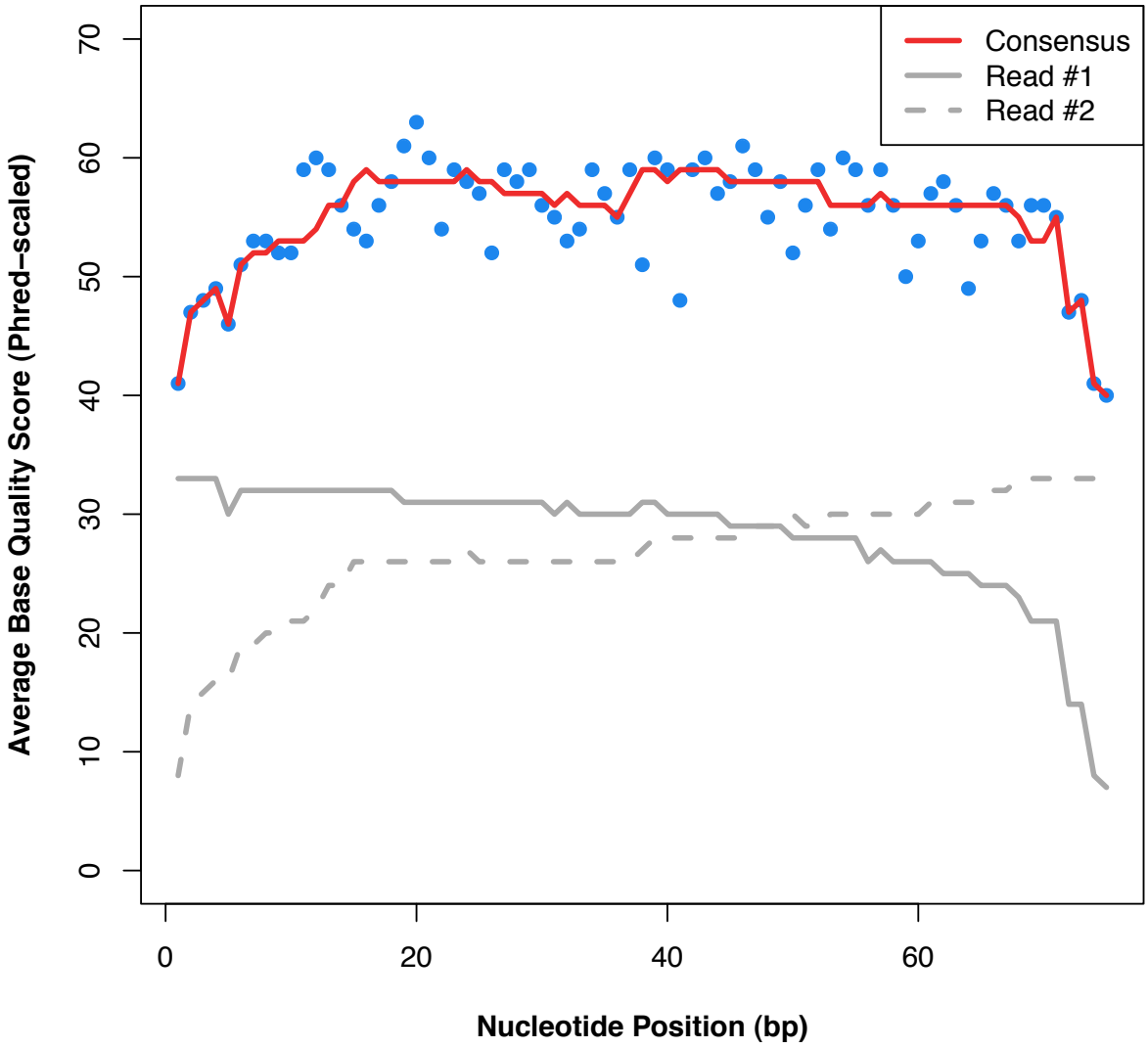

The running-median smoothed Phred-scaled per-base quality scores at each position are shown for the forward (gray line) and reverse (broken gray line) reads. Forward and reverse reads were combined, yielding a consensus sequence with a per-position error calculated as the sum of forward and reverse base quality scores for concordant base calls (i.e. error probabilities were assumed to be independent) or the highest quality score for discordant base calls. Blue dots represent the average combined score at each position and the red line indicates the running-median smoothed curve. Data presented corresponds to an analysis of reads from the input library.

Nature Methods: doi: 10.1038/nmeth.1492

Supplementary Figure 3. Sequencing of the WW Domain Diversity Library Reveals the Expected Distribution of DNA Mutations.

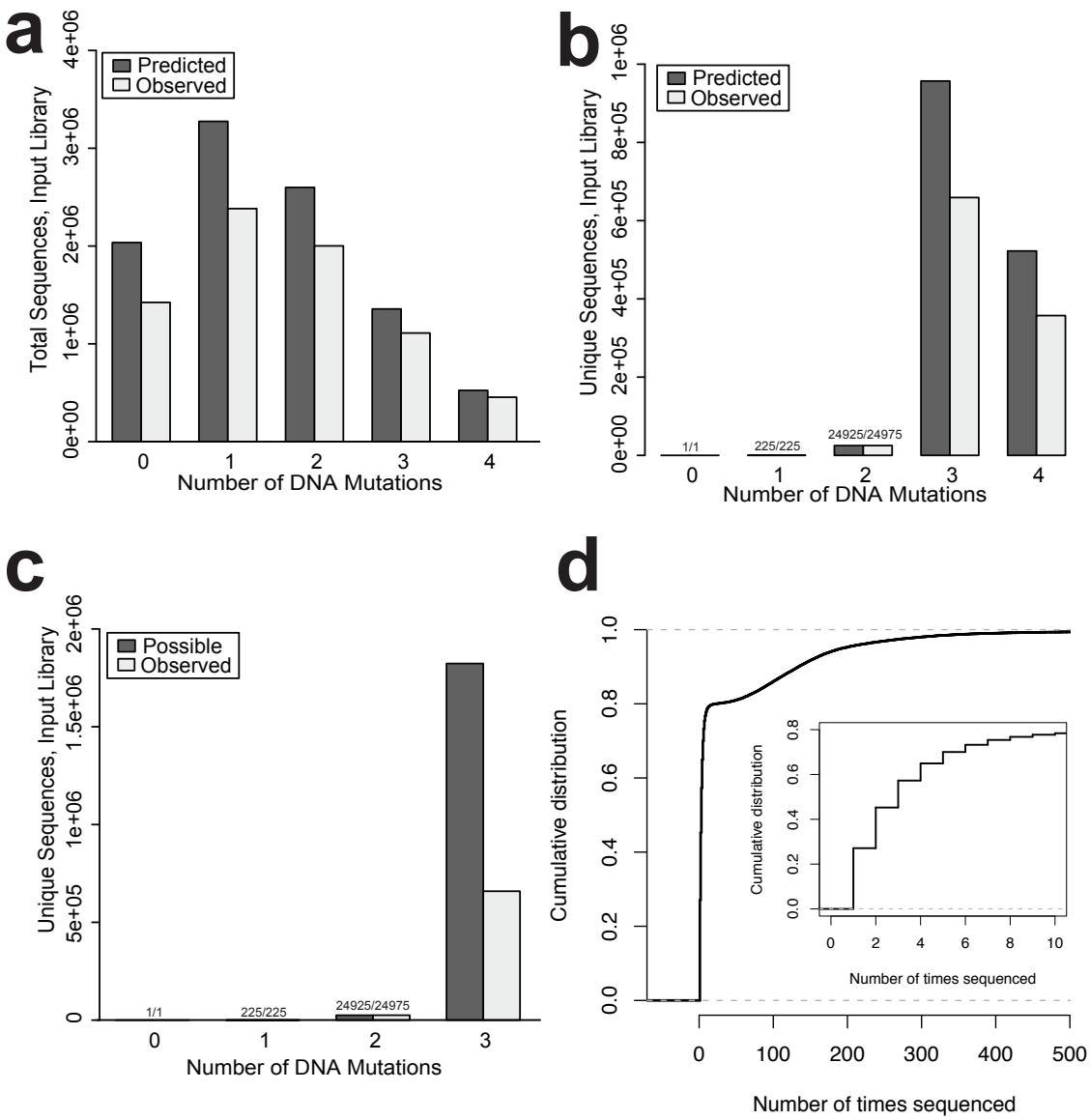

(**a**) Shown is a plot of the number of sequences with a given number of DNA mutations in the WW domain input library as determined by high-throughput sequencing. The observed distribution of mutations (light gray bars) closely matches the predicted distribution (dark gray bars). (**b**) The number of unique DNA sequences with a given number of mutations is plotted. Only one sequence, the wild type, has zero mutations. The observed distribution of mutations (light gray bars) closely matches the predicted distribution given the total number of sequences obtained (dark gray bars). (**c**) The number of unique DNA sequences with a given number of mutations is plotted. The observed distribution of mutations (light gray bars) is compared to the total number of possible sequences with a given number of mutations (dark gray bars). (**d**) A cumulative distribution of the number of times variants were sequenced is shown. The inset shows the cumulative distribution for variants sequenced up to 10 times.

Nature Methods: doi: 10.1038/nmeth.1492

Supplementary Figure 4. WW Domain Enrichment Ratio and Codon Adaptation Index are Uncorrelated.

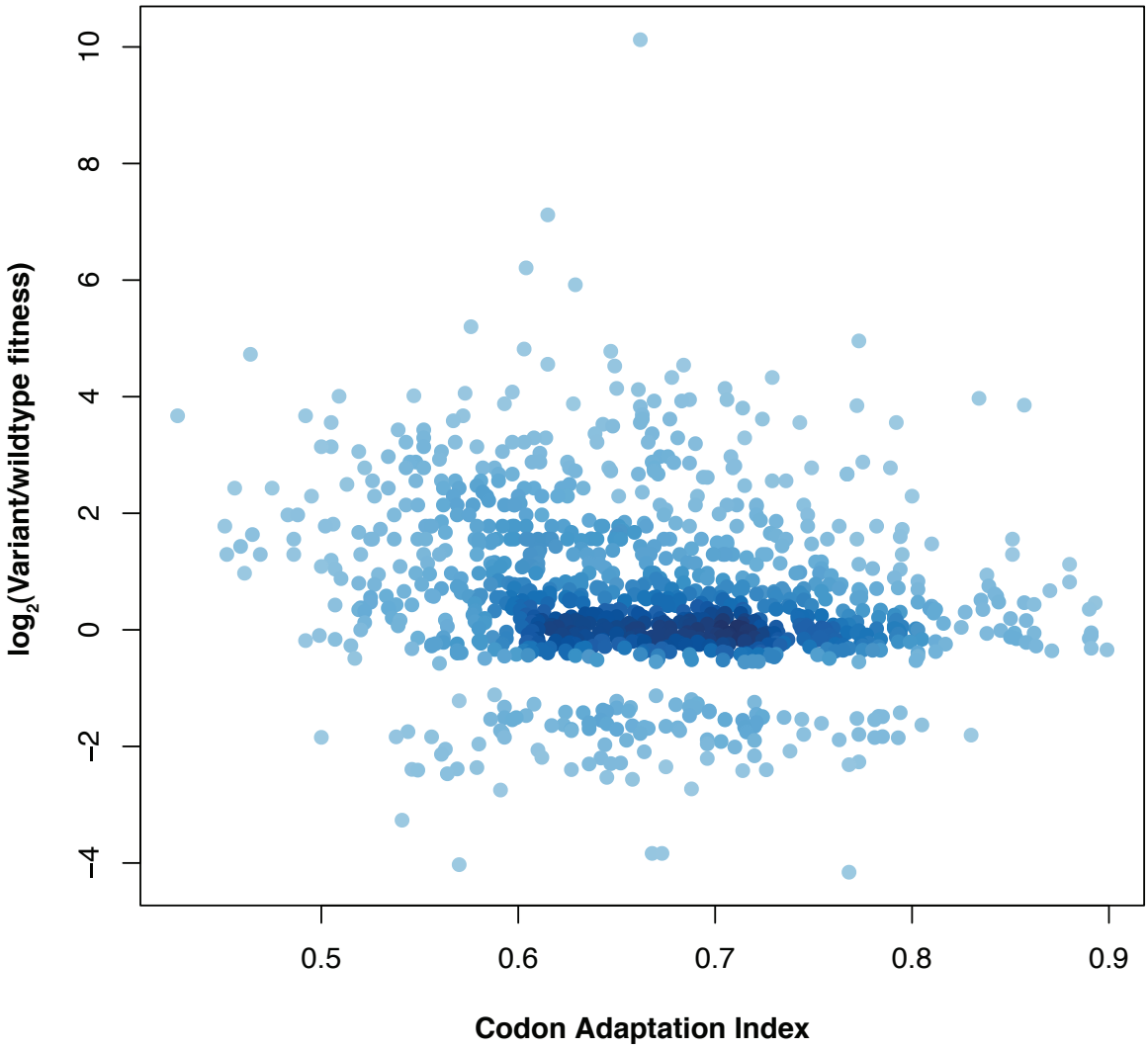

Codon adaptation index[1] scores were calculated using the CodonW algorithm for synonymous variants of the wildtype hYap65 WW domain that significantly enriched or depleted after six rounds of selection as determined by a Poisson-based test. For each variant, the codon adaptation index is plotted against the enrichment ratio.

Nature Methods: doi: 10.1038/nmeth.1492

Supplementary Figure 5. Variants Behave Similarly Across Rounds of Selection and Mutational Distance.

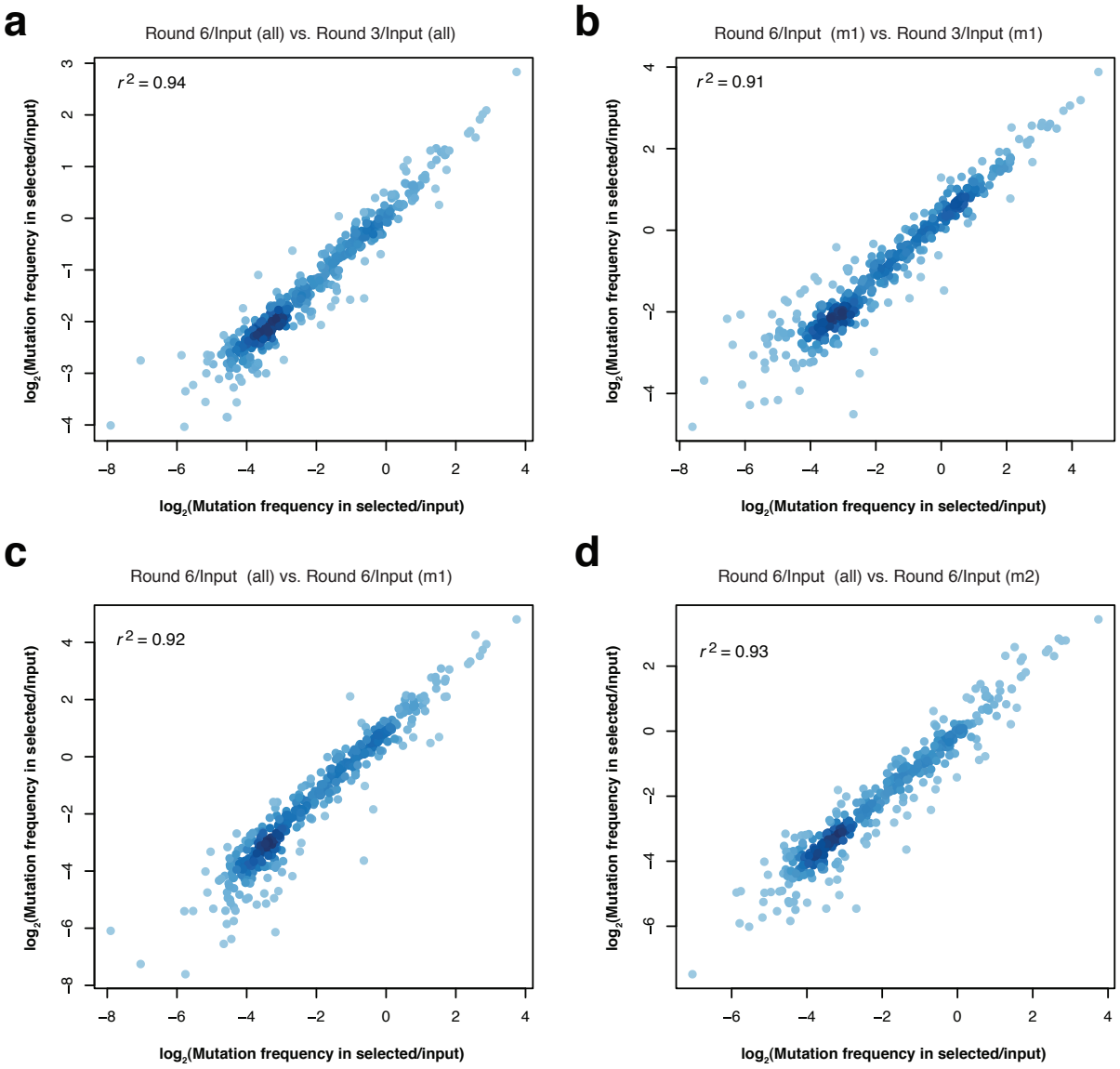

Mutational frequency (selected/input) is plotted for various subsets of data. (**a**, **b**) Mutational frequency is plotted using data from round six and data from round three (**a**) and for variants containing only single mutations (**b**). (**c**, **d**) Panel **c** shows round six enrichment ratios calculated using variants containing only one mutation versus enrichment ratios derived from all variants. Panel **d** shows round six enrichment ratios calculated using variants containing only two mutations versus enrichment ratios derived from all variants.

Nature Methods: doi: 10.1038/nmeth.1492

Supplementary Figure 6. Mutational Preferences by Position.

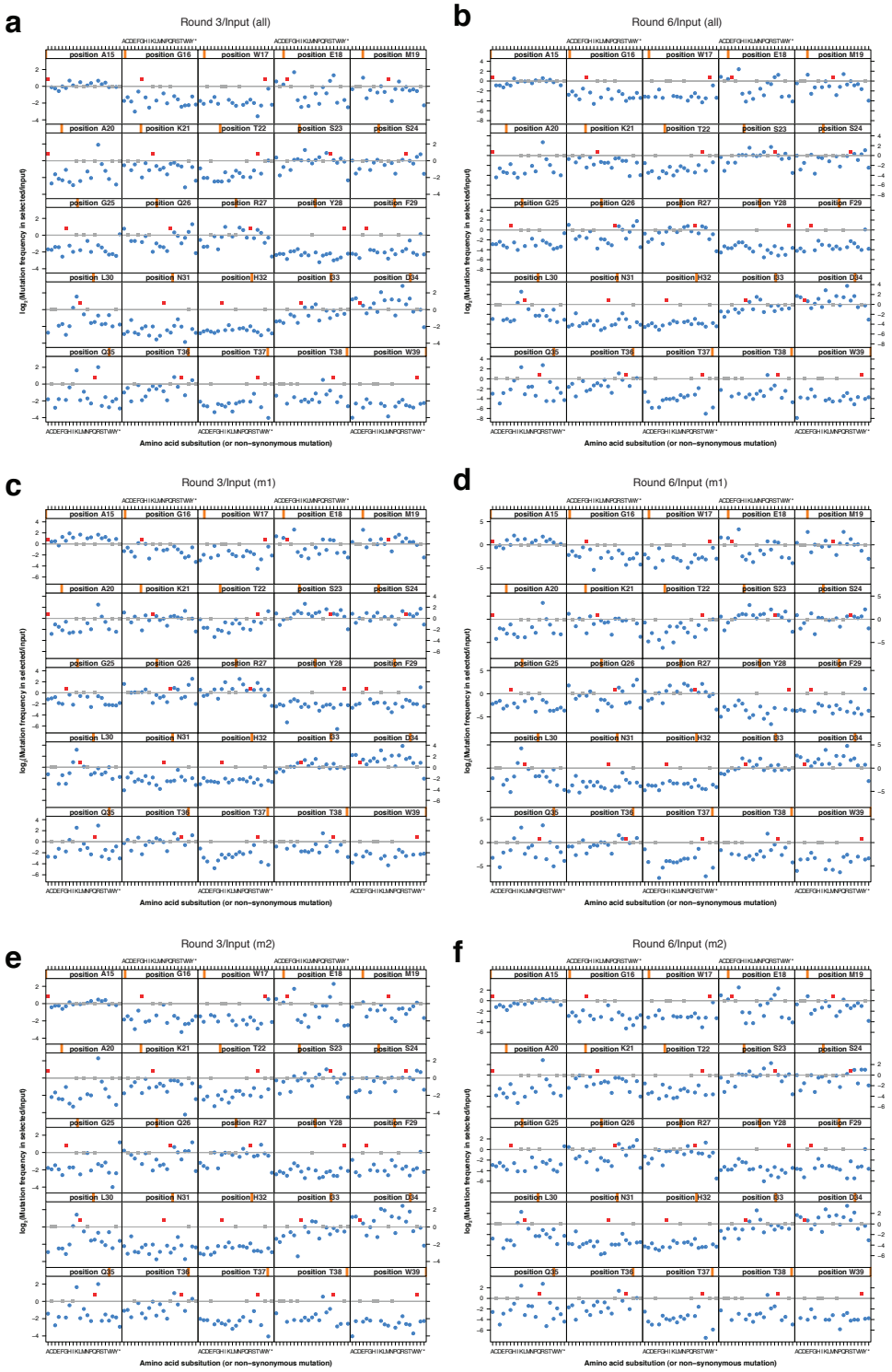

Mutational preference by position is shown for round 3 versus input (**a**, **c**, **e**) and round six versus input (**b**, **d**, **f**). Panels **a** and **b** show amino acid scans for all data, **c**, **d** show single mutant data and **e**, **f** show double mutant data. Each panel of the plot corresponds to a different position within the WW domain, indicated by the orange bar in the header. The x-axis of each panel indicates substituted amino acid while the y-axis indicates $\log_2$(enrichment ratio). Blue dots indicate a measured enrichment ratio, red dots indicate the wild type sequence (which enriched 1.7-fold) and grey dots indicate mutations not observed.

Nature Methods: doi: 10.1038/nmeth.1492

Supplementary Figure 7. Sequence Alignment of 73 WW Domains.

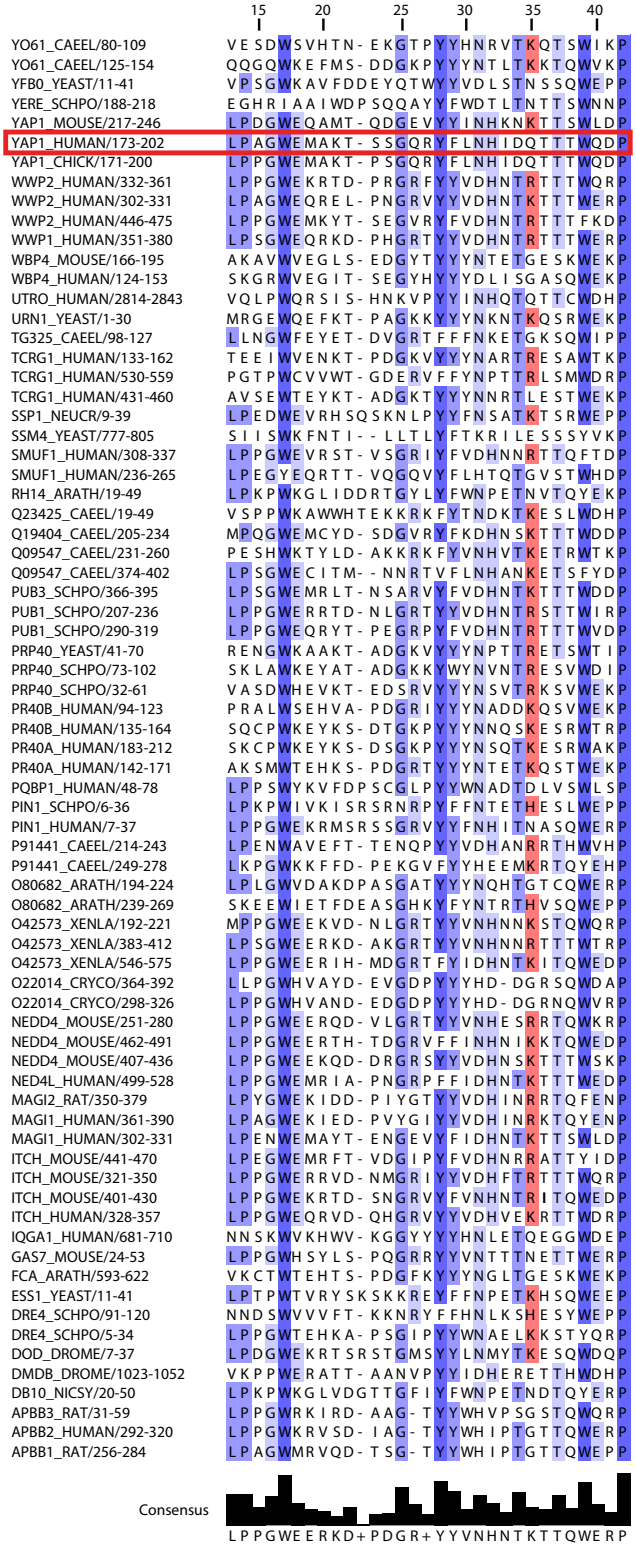

Residues 173-202 of the human Yap65 (Yap1) protein were aligned to the PFAM WW domain seed alignment (PF00397) using Jalview[2]. The hYAP65 WW domain sequence used in this study is boxed in red. Conserved positions are indicated with blue highlighting. Red highlighting indicates conservation of positively charged residues at position 35. The consensus sequence –built excluding the hYap65 sequence– is shown at the bottom, along with relative conservation at each position.

Nature Methods: doi: 10.1038/nmeth.1492

Supplementary Figure 8. Poisson-based Filtration of Enrichment Ratios.

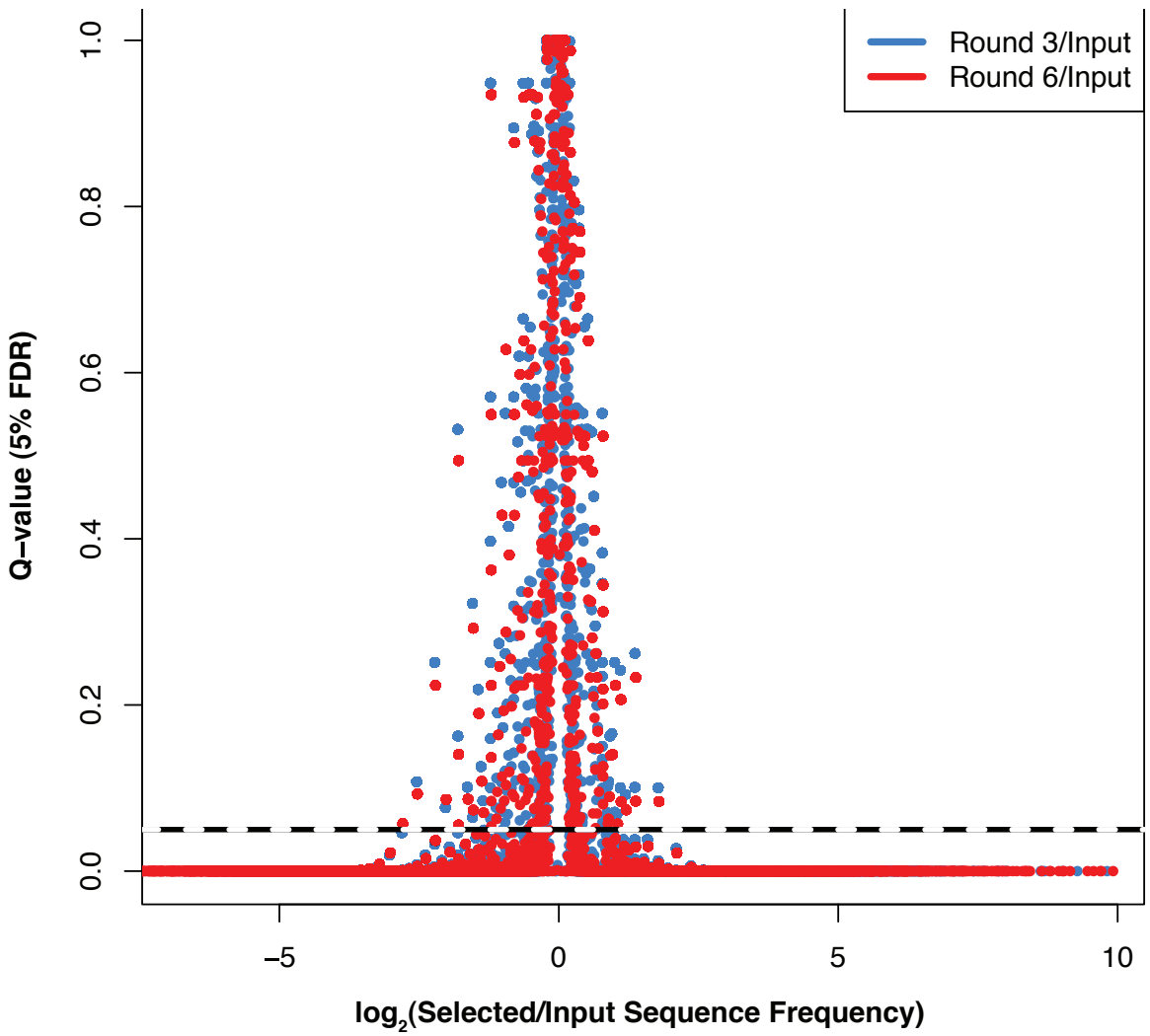

Q-values (at 5% false discovery rate) are plotted against enrichment ratios for each WW domain variant appearing in round three (red dots) and round six (blue dots). The dashed line indicates a q-value of 0.05.

Nature Methods: doi: 10.1038/nmeth.1492

Supplementary Figure 9. Validation of Five Singly Mutated WW Domain Variants.

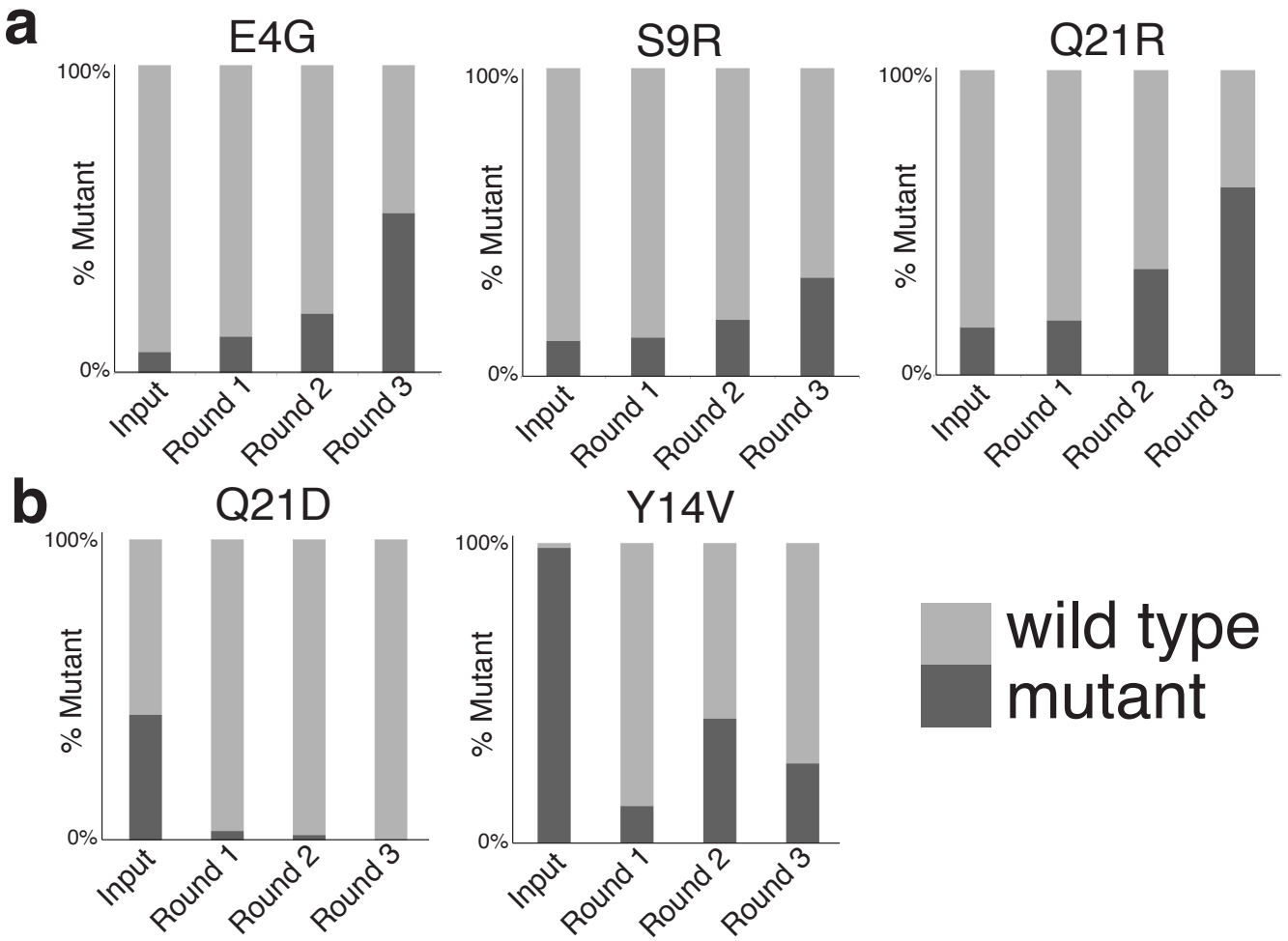

(**a**) The results of a head-to-head competition between the E4G, S9R and Q21R hYAP WW domain variants (shown in dark gray) versus wild type (shown in light gray) are shown. In each case, the mutant was seeded at 1/10th the abundance of wild type. Each of these variants were expected to enrich relative to wild type. (**b**) The results of a head-to-head competition between the Q21D and Y14V hYAP WW domain variants (shown in dark gray) versus wild type (shown in light gray) are shown. In each case, the mutant was seeded at >50% the abundance of wild type. Each of these variants were expected to deplete relative to wild type. Successive rounds of selection were analyzed using quantitative Sanger sequencing.

Nature Methods: doi: 10.1038/nmeth.1492

Supplementary Figure 10. Prediction of WW Domain Folding Energies for Enriched and Depleted Variants.

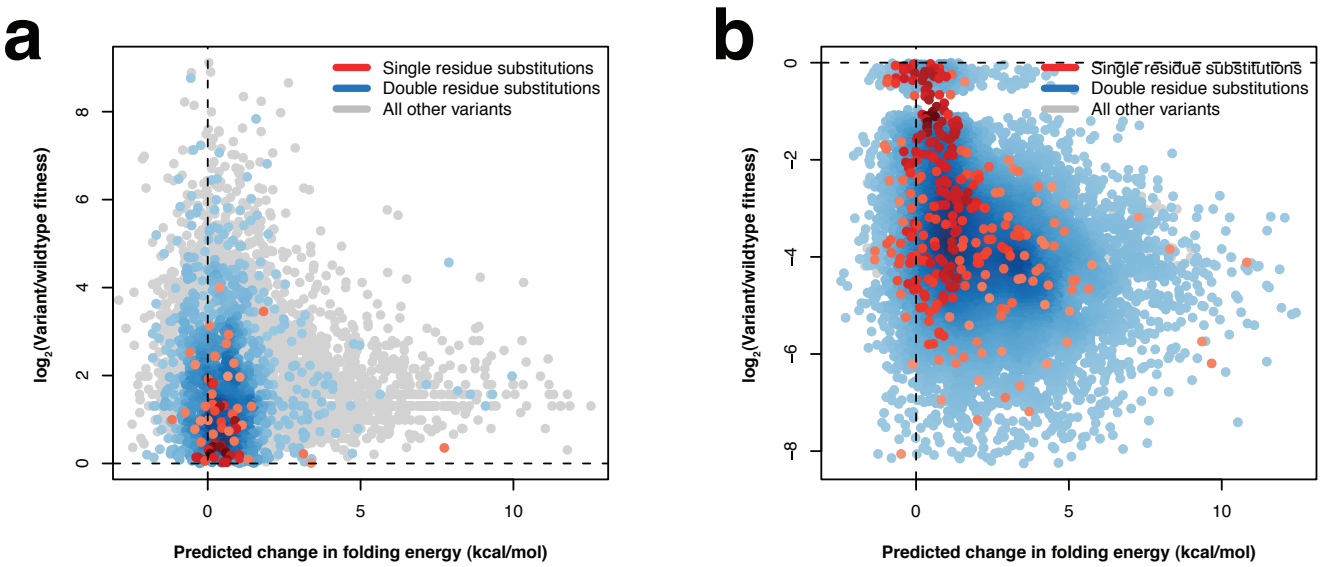

The Rosetta framework was used to calculate folding energies for the 16,363 full-length WW domain variants that significantly enriched (**a**) or depleted (**b**) after six rounds of selection. Predicted folding energies relative to the wild type WW domain energy are plotted against the observed enrichment ratio for the variants containing one (red), two (blue), or more mutations (gray).

Nature Methods: doi: 10.1038/nmeth.1492

Supplementary Figure 11. Prediction of Binding Energies for Variant WW Domains.

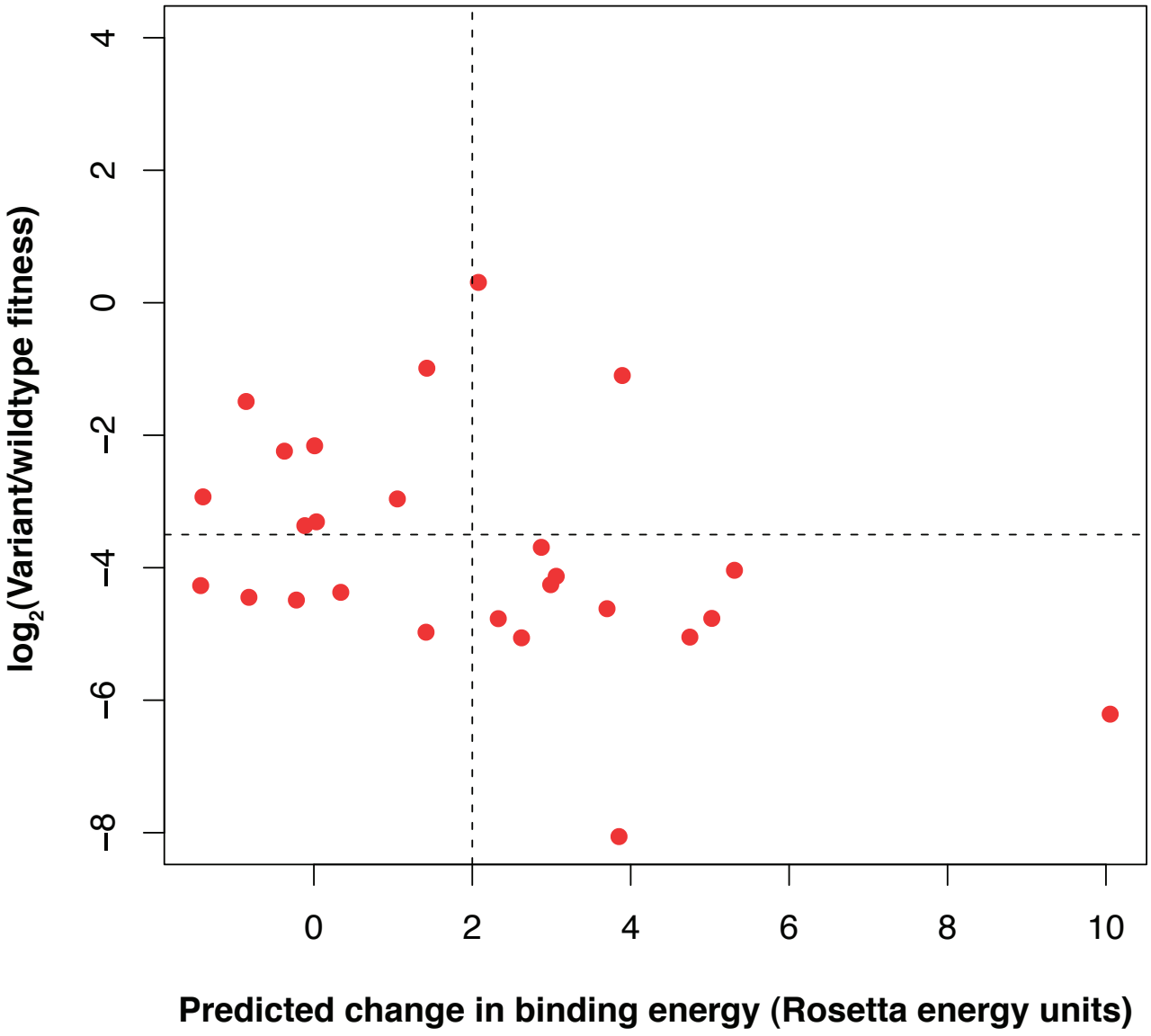

Binding energies were predicted for mutations occurring at positions that make significant contact with the ligand (Y28, L30, T37, and W39). Predicted binding energies relative to wild type are plotted against observed enrichment ratios. Dashed lines are arbitrarily placed to highlight variants with extreme negative enrichment ratios ($2^{-3.5}$ relative to wild type) or highly disruptive predicted binding energies (>2 Rosetta energy units relative to wild type).

Nature Methods: doi: 10.1038/nmeth.1492

Supplementary Table 1. Results of Quality Filtration on Raw Illumina Data.

	Raw Illumina Reads	Fuser Gapped (removed)	Fuser Low Quality (removed)	Fuser Passed	Aligner Unresolved (removed)	Aligner Passed	Filter N>3 (removed)	Filter Passed
Input	9,958,612	830,143	1,470,656	7,657,816	78,852	7,578,965	8,733	7,570,233
Round 3	11,304,570	270,897	2,126,658	8,907,018	71,038	8,835,981	4,746	8,831,236
Round 6	10,884,745	175,359	1,890,042	8,819,347	67,441	8,751,907	4,654	8,747,254

Nature Methods: doi: 10.1038/nmeth.1492

Supplementary Table 2. Primers and DNA Sequences.

ID	sequence	notes
DF-97_PCR_Long_p1F	aatgatacggcgaccaccgagatctacacgcaggagctgtcgtattccagtcag*g	HPLC purified, *= phosphorthioate
DF-97_PCR_Long_p1R	caagcagaagacggcatacgagatgcttctattatcataactgagccatggcagagg*t	HPLC purified, *= phosphorthioate
DF-97_SEQ_Short_p1F	tcccagacgacgttccactgccg	HPLC purified
DF-97_SEQ_Short_p1R	atctgagacagcatagctttacgcgggtcctg	HPLC purified
DF-97_SEQ_p1F	gctcggggatccgaattctgagatcccagac	HPLC purified
DF-97_SEQ_p1R	cggagcggtaacgttcatctgagacagcatagcttt	HPLC purified
DF-106_E4G_F	ctgccggctggttggggaatggctaaaactagt	
DF-106_E4G_R	actagttttagccattccccaaccagccggcag	
DF-106_S9R_F	tgggaaatggctaaaactaggtctggtcagcgttac	
DF-106_S9R_R	gtaacgctgaccagacctagttttagccatttccca	
DF-106_D20N_F	cttcctgaaccacatcaaccagaccaccacgtg	
DF-106_D20N_R	cacgtggtggtctggttgatgtggttcaggaag	
DF-106_Q21R_F	gaaccacatcgaccggaccaccacgtggc	
DF-106_Q21R_R	gccacgtggtggtccggtcgatgtggttc	
DF-62_WWv2F	gaattctgagatcccagacgacg	
DF-62_WWv2R	aagcttctattatcataactgagccatgg	
DF-62_T7UPv2	ctaacttccaagcggaccag	
DF-62_T7DNv2	tgagcgcatatagttcctcct	
DF-31_WWWTp1	tggtcagcgttacttcctgaaccacatcgaccagaccaccacgtggcagg	
DF-31_WWWTp2F	cggctggttgggaaatggctaaaactagttctggtcagcgttacttcctg	
DF-31_WWWTp2R	aacgttcatctgagacagcatagctttacgcgggtcctgccacgtggtgg	
DF-31_WWWTp3F	gaattctgagatcccagacgacgttccactgccggctggttgggaaatg	
DF-31_WWWTp3R	aagcttgtaactgagccatggcagaggtcggagcggtaacgttcatctgagacagca	
DF-31_W17FpF	gttccactgccggctggtttcgaaatggctaaaactagtt	
DF-31_W17FpR	aactagttttagccatttcgaaaccagccggcagtggaac	
DF-31_W39FpF	ccagaccaccacgttccaggacccgcgtaa	
DF-31_W39FpR	ttacgcgggtcctggaacgtggtggtctgg	
DF-62_WWv2F	gaattctgagatcccagacgacg	
DF-62_WWv2R	aagcttctattatcataactgagccatgg	
DF-62_WWvarV2_p1F	cagttagtcatcctgcattggcgaattctgagatcccagac	PAGE purified
DF-62_WWvarV2_p1R	ggccgtcctaaagctagtaagcttctattatcataactgagccatggcagaggtcggagcggtaacgttcatct gagacagcatagcttt	PAGE purified
DF-31_Wwvarlib_trilink	gcgaattctgagatcccagacGACGTTCCACTGCCGGCTGGTTGGGAAATGGCTAA AACTAGTTCTGGTCAGCGTTACTTCCTGAACCACATCGACCAGACCACCAC GTGGCAGGACCCGCGTaaagctatgctgtctcagatg	PAGE purified, capitalized bases are variable
WW domain sequence	gaattctgagatcccagacgacgttccactgccggctggttgggaaatggctaaaactagttctggtcagcgtt acttcctgaaccacatcgaccagaccaccacgtggcaggacccgcgtaaagctatgctgtctcagatgaac gttaccgctccgacctctgccatggctcagttatgataatagaagctt	Includes terminal EcoRI and HindIII sites

Nature Methods: doi: 10.1038/nmeth.1492

Supplementary Note 1. Rosetta Scripts.

The difference in free energy of folding was predicted using the following command line:

```
fix_bb_monomer_ddg.linuxgccrelease  -ddg::weight_file
soft_rep_design -ddg::iterations 50 -ddg::local_opt_only false -
ddg::min_cst true -ddg::mean false -ddg::min true -
ddg::sc_min_only false -ddg::ramp_repulsive true  -
ddg::minimization_scorefunction standard -ddg::minimization_patch
score12
```

To run a single trajectory of the binding simulation, the RosettaScript shown below was used:

```
<dock_design>
  <TASKOPERATIONS>
    <ThreadSequence name=thread target_sequence=""/>
    <InitializeFromCommandline name=init/>
  </TASKOPERATIONS>
  <SCOREFXNS>
  </SCOREFXNS>
  <FILTERS>
    <Ddg name=ddg confidence=0 repeats=5/>
    <Sasa name=sasa confidence=0/>
    <Rmsd name=rms confidence=0/>
  </FILTERS>
  <MOVERS>
    <Docking name=dock1 fullatom=1 local_refine=1
score_high=score12/>
    <PackRotamersMover name=thread_seq
task_operations=thread,init scorefxn=score12/>
    <Prepack name=prepacking jump_number=0/>
    <AtomTree name=at host_chain=1 pdb_num=33A/>
    <RepackMinimize name=rm repack_partner1=0 repack_partner2=0
design_partner1=0 optimize_fold_tree=0 design_partner2=0/>
  </MOVERS>
  <APPLY_TO_POSE>
  </APPLY_TO_POSE>
  <PROTOCOLS>
    <Add mover_name=thread_seq/>
    <Add mover_name=prepacking/>
    <Add mover_name=at/>
    <Add mover_name=rm/>
    <Add filter_name=ddg/>
    <Add filter_name=sasa/>
    <Add filter_name=rms/>
  </PROTOCOLS>
</dock_design>
```

Nature Methods: doi: 10.1038/nmeth.1492

In each case, the FASTA sequence of the WW variant was used to set the *target_sequence* option in the RosettaScript. RosettaScripts was invoked with the following command line:

```
rosetta_scripts -ex1 -ex2 -use_input_sc -s 1k9q.pdb -
out:file:silent default.out -out:file:silent_struct_type score -
parser:protocol thread_min.xml -nstruct 5
```

Nature Methods: doi: 10.1038/nmeth.1492

Supplementary References Cited

1. Sharp, P. M. and Li, W. H., The codon Adaptation Index--a measure of directional synonymous codon usage bias, and its potential applications. *Nucleic Acids Res.* **15** (3), 1281-1295 (1987).
2. Waterhouse, A. M., Procter, J. B., Martin, D. M., Clamp, M., and Barton, G. J., Jalview Version 2--a multiple sequence alignment editor and analysis workbench. *Bioinformatics* **25** (9), 1189-1191 (2009).

Nature Methods: doi: 10.1038/nmeth.1492